Impurity-assisted tunnelling as a probe of the donor wavefunction in n-GaAs

1990 J. Phys.: Condens. Matter 2 4439

(http://iopscience.iop.org/0953-8984/2/19/011)

J. Phys.: Condens. Matter 2 (1990) 4439–4454. Printed in the UK

Impurity-assisted tunnelling as a probe of the donor wavefunction in n-GaAs

I P Roche†, G P Whittington†, P C Main†, L Eaves†, F W Sheard†, G Wunner‡ and K E Singer§

† Department of Physics, University of Nottingham, Nottingham NG7 2RD, UK
‡ Lehrstuhl für Theoretische Astrophysik, Universität Tübingen, D-7400 Tübingen, Federal Republic of Germany
§ Department of Electrical Engineering and Electronics, UMIST, Manchester M60 1QD, UK

Received 14 September 1989, in final form 10 January 1990

Abstract. We have studied the electrical conductivity of n^+–n^-–n^+ GaAs structures in which the thickness of the n^- layer is comparable with the mean donor separation. At low temperatures, electrical conduction is dominated by a process in which electrons tunnel across the sample via shallow donor impurities close to the centre of the n^- layer. By studying the magnetoresistance of such samples we have investigated the effect of a magnetic field on the donor wavefunction in GaAs. Our measurements are compared with the approximate analytical expression for the donor wavefunction and with numerical solutions of the ground-state hydrogen wavefunctions in megatesla fields developed by astrophysicists.

1. Introduction

Theoretical studies of the effects of a magnetic field on a hydrogen atom have been motivated by their relevance to strongly magnetised objects in astrophysics (e.g. white dwarfs, neutron stars and black holes). The energy levels and wavefunctions of the hydrogen atom in megatesla fields have been calculated numerically by Rösner *et al* (1984). The results of these calculations may be applied to hydrogenic impurity states in semiconductors. The much larger Bohr radius of the impurity states means that the corresponding magnetic fields are of the order of a few teslas. Buczko *et al* (1987) have used the results of Rösner *et al* (1984) for the hydrogen ground-state wavefunction to solve the percolation problem for electron transport in strongly localised states in a direct-gap semiconductor. Their results are in good agreement with magnetoresistance data for n-type GaAs in the nearest-neighbour hopping regime in magnetic fields up to 12 T.

In this paper we report measurements of the electrical conductivity of n^+–n^-–n^+ GaAs mesa samples in which the thickness of the n^- layer is less than 0.15 μm. Previously, we have shown that the conductivity of such very short mesas is dominated by a simple tunnelling process which we have called single impurity-assisted tunnelling (Main *et al* 1986). An important feature of the impurity-assisted tunnelling process is the large and anisotropic magnetoresistance. In this paper we describe the angular dependence of the magnetoresistance of three mesa samples, of differing thicknesses, in magnetic fields up

0953-8984/90/194439 + 16 $03.50

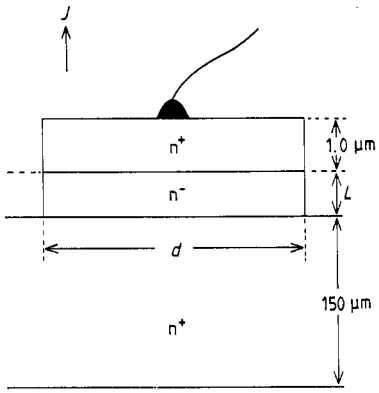

Figure 1. The structure of the n^+–n^-–n^+ GaAs mesa samples. The weakly doped 'active' layer has length L and diameter d. The direction of current flow through the sample is represented by the arrow J.

to 12 T. By analysing the angular dependence we can obtain information about the form of the impurity wavefunction in a magnetic field. The results of the investigation are in good agreement with numerical calculations of the hydrogen ground-state wavefunction in megatesla fields.

2. The sample structure

The structure of the samples studied is illustrated in figure 1. The samples were grown by MBE and mounted in standard transistor headers. Samples were grown with n^- layer thicknesses L of 129, 113 and 97.5 nm. Each sample was prepared by conventional lithography in the form of a circular mesa of diameter $d = 200\ \mu$m. Ohmic contacts were made to the top and bottom surfaces by diffusion of Au–Ge. The heavily doped n^+ regions have a total resistance of about 0.2 Ω and may be regarded as metallic contacts.

In each sample, the weakly doped n^- layer has a donor concentration N_D of 1.5 (± 0.5) $\times 10^{15}$ cm^{-3} and is expected to be moderately compensated, with acceptor concentration N_A of about 0.4×10^{15} cm^{-3}. At low temperatures the electron transport in bulk material of such a low impurity concentration is by electrons hopping between the localised donor states (Emel'yanenko *et al* 1974). In our samples, however, L is less than twice the mean separation of the donor impurities, i.e.

$$L < 2N_D^{-1/3}.$$

In such very short mesas, it becomes favourable for electrons to tunnel elastically across the sample via shallow donors situated close to the centre of the layer rather than hopping between several donor sites.

3. Theory of impurity-assisted tunnelling conduction

The conduction process is treated as two successive transitions, from the left-hand (LH) n^+ contact into an impurity state in the n^- layer and then from the impurity state into

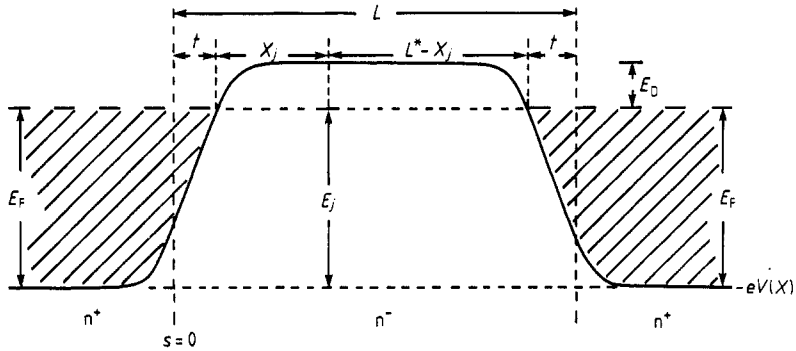

Figure 2. The electron potential energy $-eV(X)$ through a cross section of the mesa samples. E_F is the Fermi energy in the metallic n^+ layers. E_j and X_j are the energy and position respectively of a donor state j in the active layer. The length of the potential barrier created by the n^- region is reduced by a distance t at each n^+–n^- interface owing to screening effects. See text for the explanation of the other symbols.

the right-hand (RH) n^+ region (figure 2). We label the electron states in the LH Fermi sea by wavevectors $\boldsymbol{k}$ (energy E_k), in the RH Fermi sea by $\boldsymbol{p}$ (energy E_p) and the impurity states by a site index j (energy E_j). Introducing the corresponding transition rates W_{kj} ($=W_{jk}$) and W_{pj} ($=W_{jp}$), the rate equations for the occupancies f_k and f_j of the LH and impurity states are

$$\dot{f}_k = -\sum_j (f_k - f_j)W_{kj} \tag{1}$$

$$\dot{f}_j = -\sum_k (f_j - f_k)W_{kj} - \sum_p (f_j - f_p)W_{pj}. \tag{2}$$

Under steady-state conditions, $\dot{f}_j = 0$. This gives

$$f_j = \left(\sum_k f_k W_{kj} + \sum_p f_p W_{pj}\right) \Big/ [(\tau_{Lj})^{-1} + (\tau_{Rj})^{-1}] \tag{3}$$

where $1/\tau_{Lj} = \Sigma_k W_{kj}$ and $1/\tau_{Rj} = \Sigma_p W_{pj}$. By identifying $1/\tau_{Lj}$ as the decay rate for an electron tunnelling from impurity site j into unoccupied LH states, we may write

$$1/\tau_{Lj} = 1/\tau_L(X_j) = \nu T_L(X_j)$$

where ν is the attempt rate of an electron in the bound impurity state and $T_L(X_j)$ is the transmission coefficient from the impurity state at position X_j into LH continuum states (see figure 2). Similarly $1/\tau_{Rj}$ gives the decay rate into RH states.

The current (from LHS to RHS) is given by $I = e\Sigma_k \dot{f}_k$, where $-e$ is the electronic charge. Use of equations (1) and (3) gives, after some manipulation,

$$I = -e \sum_j F_j/(\tau_{Lj}^{-1} + \tau_{Rj}^{-1}) \tag{4}$$

where

$$F_j = \sum_{k,p} (f_k - f_p)W_{kj}W_{pj}.$$

The expression for I is to be evaluated when there is a small voltage bias V across the

structure which raises the RH Fermi level by eV with respect to the LH Fermi level. Since the electric field in the conducting n^+ contacts is small, we may take f_k to be an equilibrium Fermi–Dirac distribution at temperature T:

$$f_k \equiv f^0(E_k) = \{\exp[\beta(E_k - E_F)] + 1\}^{-1}$$

where $\beta = 1/k_B T$ and E_F is the Fermi energy in the contacts. Thus

$$f_p = f^0(E_p - eV) = \{\exp[\beta(E_p - E_F - eV)] + 1\}^{-1}.$$

We may now evaluate equation (4) for the current assuming that, at low temperatures, the tunnelling is elastic ($E_k = E_j = E_p$) and the bias is small ($eV \ll E_F$). This gives a linear I/V dependence and a conductance $G = I/V$:

$$G = -e^2 \sum_j \frac{\tau_{Lj}^{-1}\tau_{Rj}^{-1}}{\tau_{Lj}^{-1} + \tau_{Rj}^{-1}} \frac{\partial f^0(E_j)}{\partial E_j}. \tag{5}$$

To take account of a distribution of impurity energies, we average over E_j using a density $D(E_j)$ of states, which is the number of impurities per unit energy range per unit volume. This procedure is independent of the average over spatial sites which is performed by converting the sum over j into a volume integral. Thus

$$\sum_j \rightarrow \int_0^{L^*} A \, \mathrm{d}X_j \int D(E_j) \, \mathrm{d}E_j$$

where L^* is the effective width of the n^- region (see figure 2) and A the area of cross section. This gives

$$G = e^2 D(E_F) \int_0^{L^*} \frac{\mathrm{d}X}{\tau_L(X) + \tau_R(X)} \tag{6}$$

where, at low temperatures, we have taken the derivative of the Fermi function to be a delta function. In section 4 the relation between L and L^* is determined.

In the absence of a magnetic field the transmission coefficients T_L and T_R will be dominated by the decay of the s-state impurity wavefunction. Hence we can write

$$T_L = K \exp(-2X/a_0) \qquad T_R = K \exp[-2(L - X)/a_0]$$

where a_0 is the effective Bohr orbit radius, about 10 nm in GaAs, and K is a prefactor which may be taken to be constant. The integrand in equation (6) then has a sharp peak at $X = L^*/2$ of half-width $\Delta X \sim a_0$ showing that only impurities near the middle of the active layer contribute to the conduction. On performing the integral we find that

$$G = -e^2 A D(E_F) K \nu a_0 \exp(-L^*/a_0) \{\tan^{-1}[\exp(-L^*/a_0)] - \pi/4\}.$$

For our specimens, $L^* \gg a_0$; so this reduces to

$$G = e^2 A D(E_F) K(\pi/4) \nu a_0 \exp(-L^*/a_0). \tag{7}$$

Since the electron transitions do not require the absorption or emission of a phonon, the impurity-assisted tunnelling process is independent of temperature. In our samples, in zero magnetic field, the measured resistance is predominantly the resistance of the n^+ layers and contacts. In a large magnetic field the donor wavefunctions, and hence the tunnelling conductivity, are severely restricted, particularly in the transverse direction. The measured sample resistance is then principally that of the active layer.

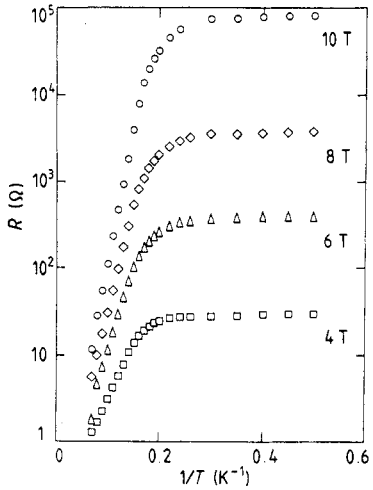

Figure 3. Measured resistance against T^{-1} for a mesa of nominal length $L = 129$ nm at various magnetic fields ($\boldsymbol{B} \perp \boldsymbol{J}$).

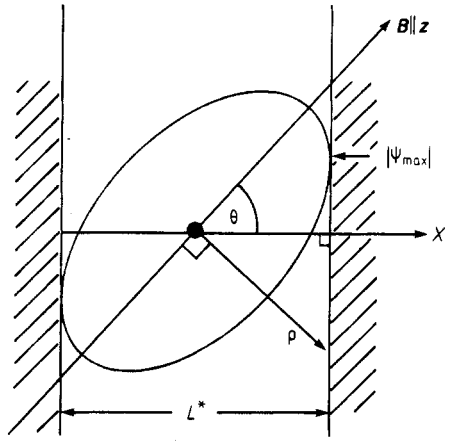

Figure 4. A schematic illustration of the impurity-assisted tunnelling process in a magnetic field $\boldsymbol{B}$, where $\boldsymbol{B}$ is oriented at an angle θ with respect to the sample axis: ——, a single contour of constant wavefunction amplitude for a donor situated in the centre of the n^- layer. $|\psi_{max}|$ is the maximum value of the donor wavefunction at the n^+–n^- boundary (see section 6).

4. Impurity-assisted tunnelling in a magnetic field

In figure 3 the resistance of a sample of thickness $L = 129$ nm in transverse ($\boldsymbol{J} \perp \boldsymbol{B}$) magnetic fields of between 4 and 11.5 T is shown as a function of inverse temperature. At temperatures higher than about 5 K the electrical conductivity of the sample shows an activated dependence on temperature. The activation energy, in the temperature range $T = 18$ K to $T = 6$ K, increases from 4.6 ± 0.3 meV in a magnetic field of strength $B = 8$ T to 6.1 ± 0.3 meV for $B = 11.5$ T. The magnitude of the activation energy is about half the ionisation energy for an isolated donor impurity in a magnetic field of 10 T predicted from numerical studies of the hydrogen atom by Rösner *et al* (1984). This suggests that the electrical conductivity of the sample above about 5 K is dominated by thermally ionised donor electrons in the weakly doped layer. The 'freeze-out' of the activated conduction mechanism at lower temperatures reveals the temperature-independent impurity-assisted tunnelling process.

The effect of a magnetic field on electron transport between localised impurity states in a weakly doped semiconductor has been reviewed by Shklovskii and Efros (1984). Their expression for the asymptotic form of the donor impurity wavefunction in a strong magnetic field may be applied to the much simpler case of single-impurity-assisted tunnelling.

For a donor in an isotropic semiconductor the Hamiltonian has the same form as for a hydrogen atom with the mass of the electron replaced by the effective mass m^* and the Coulomb term multiplied by the inverse of the lattice dielectric constant. The effect of the magnetic field is to introduce an extra term $e^2B^2\rho^2/8m^*$ into the Hamiltonian, where ρ is the cylindrical radius ($\boldsymbol{\rho} \perp \boldsymbol{B}, z \| \boldsymbol{B}$) which acts to pull the electron towards an

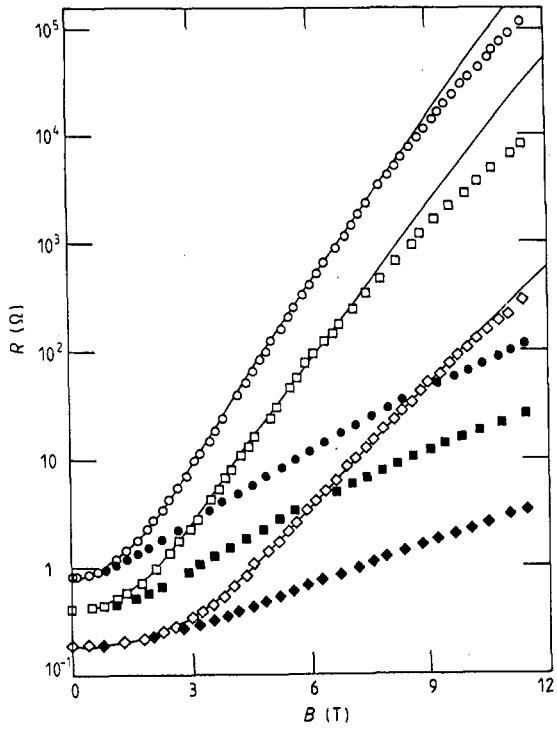

Figure 5. The resistance R of the L = 129 nm (○, ●), 113 nm (□, ■) and 97.5 nm (◇, ◆) samples in transverse (○, □, ◇) and longitudinal (●, ■, ◆) magnetic fields B at a temperature of 2 K: ——, best agreement obtained between the transverse magnetoresistance data and the theory (equation (10)).

axis z passing through the donor ion and parallel to the magnetic field (figure 4). For $\rho \gg \lambda^2/a_0$, where $\lambda^2 = \hbar/eB$, the wavefunction is dominated by the magnetic field. In the direction perpendicular to the magnetic field the wavefunction varies as

$$\psi(\rho) \propto \exp(-\rho^2/4\lambda^2) \tag{8}$$

for $z = 0$.

An expression for the conductivity of the impurity-assisted tunnelling process in a transverse magnetic field ($\theta = 90°$) may now be derived. In a strong transverse magnetic field $\boldsymbol{B}$ (perpendicular to the current flow), the asymptotic form of the wavefunction shows that

$$T_L = K' \exp(-X^2/2\lambda^2) \qquad T_R = K' \exp[-(L^* - X)^2/2\lambda^2]$$

where $\lambda = (\hbar/eB)^{1/2}$ is the magnetic length and K' a constant prefactor. The form of the integral in equation (6) shows that the contributing impurities lie within a distance $\Delta X \sim 2\lambda^2/L^*$ of the centre of the active layer. Since $L^{*2}/2\lambda^2 \gg 1$, the integral may be approximately evaluated and gives

$$G_\perp = e^2 A D(E_F) K' \nu(\pi\lambda^2/L^*) \exp(-L^{*2}/8\lambda^2) \tag{9}$$

and the magnetic field dependence of the resistance is of the form

$$R_\perp(B) \propto B \exp(L^{*2}eB/8\hbar). \tag{10}$$

As in the zero-field case, the exponent in the conductance is proportional to the impurity wavefunction squared at a distance $L^*/2$ from the donor site.

From equation (10), a plot of $\log R_\perp$ versus B should be approximately linear, the slope being proportional to L^{*2}. Examples of such plots are shown in figure 5 for samples

of length $L = 129$, 113 and 97.5 nm in transverse and longitudinal magnetic fields at $T = 2$ K. At such low temperatures the sample resistance is independent of temperature (see figure 3). The full curves in figure 5 represent a fit to the transverse magnetoresistance of the three samples with a function of the form

$$R_\perp(B) = R_0 + R_1 B \exp(\xi B) \tag{11}$$

where R_0 is the zero-field resistance, R_1 a constant of proportionality and ξ approximately the slope of the graph. From equation (10) the effective length of the n^- layer is given by

$$L^* = (8\xi\hbar/e)^{1/2}. \tag{12}$$

In general, L^* will not be the same as the length of the n^- layer as grown. The width of the potential barrier, created by the n^- layer, is reduced by the diffusion of the free electrons from the n^+ regions at each interface as shown in figure 2. The effective length $L^* = L - 2t$, where t is the width of the diffusion region.

The diffusion width may be estimated by studying the band bending in the vicinity of the interface $s = 0$, between a heavily doped n^+ region ($s < 0$) and a lightly doped region ($s > 0$) in the Thomas–Fermi approximation. The coordinate s is used to define distances measured relative to the doping discontinuity which we take as $s = 0$. If for $s > 0$ the fixed charge is neglected, the space charge arises only from conduction electrons with local density $n(s)$ and the local Fermi energy $E_F(s) = (\hbar^2/2m^*)(3\pi^2 n(s))^{2/3} \to 0$ as $s \to \infty$. For $s < 0$, $E_F(s) \to E_{F0} = (\hbar^2/2m^*)(3\pi^2 N_D)^{2/3}$ as $s \to -\infty$, where N_D is the uncompensated donor density in the n^+ region. Poisson's equation for the electrostatic potential $V(s)$ is

$$d^2V/ds^2 = -\rho(s)/\varepsilon_r\varepsilon_0 \tag{13}$$

where $\rho(s) = -en(s)$ for $s > 0$ and $-e[n(s) - N_D]$ for $s < 0$, and ε_r is the dielectric permittivity of GaAs. If the zero of potential is taken to be the conduction band edge as $s \to \infty$, then the condition of constancy of the Fermi level gives

$$E_F(s) - eV(s) = 0. \tag{14}$$

Equations (13) and (14) give rise to a non-linear equation for $E_F(s)$ or $V(s)$, the first integral of which gives

$$dE_F/ds = \begin{cases} -\gamma^{1/2}[E_F^{5/2} - E_{F0}^{5/2} - \frac{5}{2}E_{F0}^{3/2}(E_F - E_{F0})]^{1/2} & (s < 0) \\ -\gamma^{1/2}E_F^{5/4} & (s > 0) \end{cases}$$

where $\gamma = 8/15E_{F0}^{1/2}L_{TF}^2$ and $L_{TF} = (2E_{F0}\varepsilon_r\varepsilon_0/3N_De^2)^{1/2}$ is the Thomas–Fermi screening length. Continuity of dE_F/ds at $s = 0$ then requires

$$E_F(0) = \tfrac{3}{5}E_{F0}. \tag{15}$$

Further integration with the boundary condition (15) then gives, for $s > 0$,

$$E_F(s) = eV(s) = 900L_{TF}^4E_{F0}/[x + (1500)^{1/4}L_{TF}]^4. \tag{16}$$

If the fixed charge in the lightly doped n^- region is not neglected, then equation (16) is not accurate for large values of s since, in a partially compensated sample, the Fermi level must then pass asymptotically through the shallow donor level at an energy E_D below the band edge, as shown in figure 2. Thus we can take the screening length t to be

Table 1. The effective length L_C^* derived from the sample capacitance, the effective length $L - 2t$ derived from screening theory, and effective length L_B^* derived from the transverse magnetoresistance of the samples.

L (nm)	C (pF)	L_C^* (nm)	$L - 2t$ (nm)	L_B^* (nm)
129 ± 1	140 ± 4	92 ± 5	92 ± 4	75.2 ± 0.2
113 ± 1	153 ± 4	85 ± 5	75 ± 4	71.9 ± 0.2
97.5 ± 1	—	—	60 ± 4	63.2 ± 0.2

given approximately by the distance at which the electron potential energy $-eV(t) = -E_D$, i.e.

$$t/L_{TF} = (900E_{F0}/E_D)^{1/4} - (1500)^{1/4}. \tag{17}$$

For $N_D = 1.5\ (\pm 0.5) \times 10^{18}\,\text{cm}^{-3}$, $E_{F0} = 70 \pm 15\,\text{meV}$ and, taking $E_D = 5.7\,\text{meV}$, the total screening length is estimated to be $2t = 30$–$40\,\text{nm}$. As equation (14) is only valid for electrostatic potentials that vary slowly in comparison with the wavelength $\lambda_F = 30\,\text{nm}$ of electrons at the Fermi energy in the metallic layer, equation (17) is only a rough approximation of the screening length.

The capacitance of the samples is a measure of the dielectric width of the active layer. We measured the capacitance C of samples of diameter $400\,\mu\text{m}$ using a low-level capacitance bridge with excitation frequency between 25 and 150 kHz. Measurements were made at high transverse magnetic fields where the large magnetoresistance allows a reasonable phase angle in the capacitance bridge circuit. The results are given in table 1, together with the derived active lengths L_c^*, given by the inverse capacitance per unit area and $L - 2t$. The active length L_B^*, derived from the transverse magnetoresistance resistance of the samples (equations (11) and (12)) is also shown. Note that L_C^* and L_B^* are experimental estimates of the real active length of the sample L^* as shown in figure 2.

The agreement between L_B^* and our estimate of $L - 2t$ is very good, particularly for the two shorter samples. At high magnetic fields ($B > 8\,\text{T}$) the resistance of the two larger samples shown in figure 5 is less than the theoretical curves predict. A possible mechanism for this is discussed later.

The longitudinal magnetoresistance of these samples is harder to treat analytically. The shrinkage of the hydrogen atom in the longitudinal direction, arising from the increased binding energy of the state, is small. Shklovskii and Efros (1984) suggest that the wavefunction in the z direction is given by

$$\psi_{\parallel} \propto \exp(-z/a_B) \tag{18}$$

where a_B is the magnetic-field-dependent Bohr radius:

$$a_B = \hbar^2/[2m^*E_0(B)]^{1/2} \tag{19}$$

and $E_0(B)$ is the binding energy. Rösner *et al* (1984) have calculated the dependence of E_0 on B for the hydrogen atom. If their results are substituted into equations (18) and (19), the effective lengths derived from the longitudinal magnetoresistance of the three samples are very similar, about $110 \pm 10\,\text{nm}$. However, the analytical expression for the

wavefunction in the z direction suggested by Shklovskii and Efros has a considerably stronger dependence on B than the numerical solutions of Rösner *et al* (1984) do.

5. The hydrogen atom in a magnetic field

Rösner *et al* (1984) have calculated the wavefunctions and energies for a hydrogen atom in an arbitrary magnetic field. Measuring the energies in effective rydbergs and lengths in effective Bohr radii the Hamiltonian for the problem for spin-down states is given by

$$H = -\nabla^2 - 2/r + 2\beta l_z + \beta^2\rho^2 - 2\beta \tag{20}$$

where the magnetic field points along the z direction, $\rho^2 = x^2 + y^2$ and $r^2 = x^2 + y^2 + z^2$. The magnetic field parameter β is given by

$$\beta = B/B_0. \tag{20a}$$

Here B is the magnetic field strength in teslas and

$$B_0 = B_H(a/a_0)^2$$

where $a = 0.53$ nm is the Bohr radius of hydrogen, and $B_H = 4.7 \times 10^5$ T. Therefore, taking $a_0 = 10$ nm for donor states in GaAs, the value of B_0 is 13.2 T. Because of the non-integrable nature of the Hamiltonian (20) its eigenfunctions can only be determined numerically. Details of such calculations have been described by Rösner *et al* (1984). However, in order to obtain highly accurate values of the wavefunctions also in regions $(5–10)a_0$ away from the donor site, it turned out to be necessary to modify the numerical method; instead of directly integrating, in the spherical expansion of the states, the system of coupled differential equations resulting from the projection of Schrödinger's equation on the different angular momentum components we chose to expand the radial functions in terms of a complete orthogonal basis set (of Sturmian type) and to diagonalise the Hamiltonian matrix. The results presented here were obtained using a set of 3600 basis functions. The computations were performed on the Cray 1 at the University of Stuttgart.

In figure 6 the ground-state (1s) wavefunction is shown for magnetic field parameters $\beta = 0.4, 0.6$ and 0.9, corresponding to $B = 5.3, 7.9$ and 11.9 T. The full curves represent surfaces of constant $|\psi|^2$ ($|\psi|^2 = 10^{-1}, 10^{-2}, 10^{-3}, \ldots$, up to 10^{-10} from the donor site outwards). The length scale has units a_0, where $a_0 = 10$ nm for the donor states. The diagrams illustrate the stronger and stronger deformation of the impurity wavefunction, with the regions in the vicinity of the nucleus (donor site) being influenced to a much lesser extent than those farther out.

The numerical solutions of the ground-state wavefunction in the transverse ($z = 0$) direction are shown in the full curves in figure 7 on a plot of $\log|\psi_\perp|$ versus ρ^2 for $\beta = 0–1.1$ at distances $0 < \rho < 8a_0$. In figure 7, most of the wavefunction is concentrated within a few Bohr radii of the donor site. Therefore, normalisation of the wavefunction does not significantly affect its asymptotic form, as may be seen from the agreement between the numerical and analytical solutions. At large distances from the donor site ($\rho > 5a_0$), $|\psi_\perp|$ approaches the 'strong'-field asymptotic form, represented by the straight broken lines, suggested by Shklovskii and Efros (equation (8)). At a distance corresponding to half the effective length of our samples ($3a_0 < \rho < 4a_0$), the constriction of the wavefunction if β is increased from 0.4 to 1.1 is about half that predicted

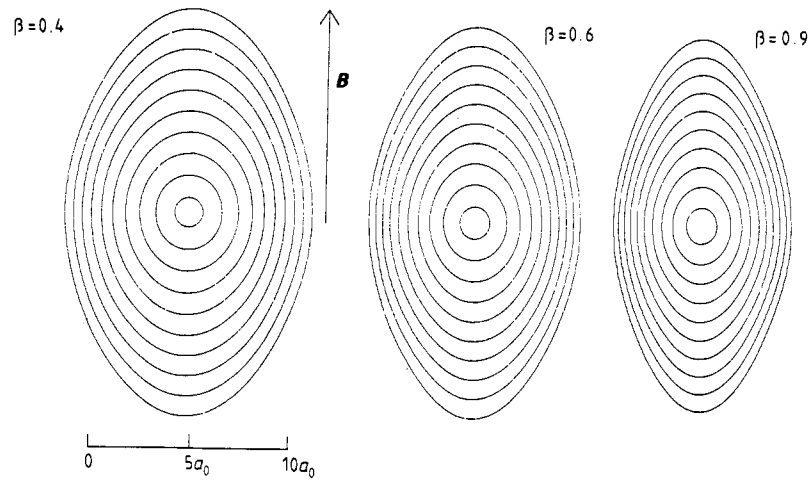

Figure 6. Some numerical solutions of the ground-state hydrogen-like wavefunction in a magnetic field: ——, contours of constant $|\psi|^2$. The magnetic parameter β is proportional to the field strength (equation (20*a*)).

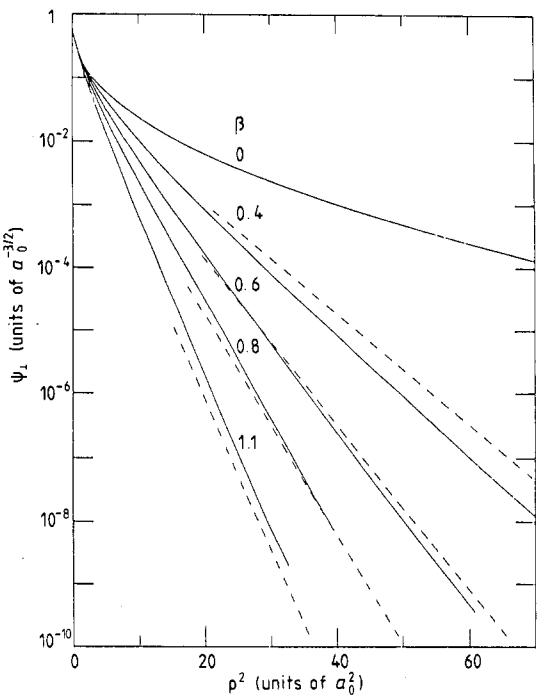

Figure 7. The hydrogen-like wavefunction for different β versus ρ^2, where ρ is the distance from the donor site in the transverse ($z = 0$) direction: ---, dependence predicted by equation (8).

by equation (18). Consequently, the effective length L_B^* derived from the transverse magnetoresistance is about 10% larger for each sample than that given in table 1.

In the longitudinal direction ($\rho = 0$) the shrinkage of the wavefunction due to the magnetic field is very much less than would be expected from equations (18) and (19).

For example $|\psi_\parallel|^2$ is reduced to 80% of the zero-field value for $z = 3a_0$, and 40% of the zero-field value for $z = 4a_0$ if a magnetic field of $\beta = 0.8$ is applied. Rösner *et al* (1984) have calculated that $E_0(\beta = 0.8) = 1.8E_0(\beta = 0)$; the corresponding decrease in the Bohr radius (equation (19)) gives a reduction in $|\psi_\parallel|^2$ (equation (18)) that is six times larger at these distances.

The longitudinal magnetoresistance of the three mesa samples shown in figure 5, $R_\parallel(\beta = 0.8)/R_\parallel(\beta = 0) \simeq 80$, is larger, by a factor of about 40, than can be explained by the calculated shrinkage of the wavefunction. A possible explanation for this discrepancy would be an increase in L^* at high B due to the rise in the donor binding energy, leading to a decrease in t (equation (17)). However, $R_\perp(B)$ would then be expected to rise much faster than $\log R_\perp(B) \propto B$. Since any increase in L^* would presumably be independent of the direction of B, the angular dependence of the magnetoresistance may be used to investigate further the impurity-assisted tunnelling process and the shape of the donor wavefunction.

6. The angular dependence of impurity-assisted tunnelling

The angular dependence of the resistance $R(\theta)$ of the three mesa samples at 4.2 K in several fixed magnetic fields, corresponding to $\beta = 0.4$–0.8, is shown in figure 8. Here θ is the angle between the current and field directions. A small series resistance of about 0.2 Ω has been subtracted from the measured sample resistance. The subtracted resistance is the temperature-independent resistance of the sample as it is cooled from room temperature to 4.2 K. This is taken to be the resistance of the n^+ layers and electrical contacts. The remaining resistance $R(\theta)$ is, therefore, the resistance of the active layer only. The subtraction of the series resistance is only significant for the shortest mesa at the lowest magnetic fields shown.

At each magnetic field, $R(\theta)$ passes through a minimum, corresponding to the longitudinal magnetoresistance $R_\parallel$, and a maximum, corresponding to the transverse magnetoresistance $R_\perp$. The rise in the magnetoresistance anisotropy $R_\perp/R_\parallel$ as the sample thickness is increased is due to the greater deformation of the impurity wavefunction at larger distances from the donor site, as may be seen in figure 6.

The dominant term in the sample conductance (equations (7) and (9)) is the magnitude of $|\psi|^2$ at a distance $L^*/2$ from the donor site, i.e.

$$G \propto |\psi_{\max}(L^*/2)|^2 \tag{21}$$

where $\Psi_{\max}$ is the largest value of ψ along the n^+–n^- boundary for a donor situated in the centre of the sample. Therefore, if any dependence of the pre-exponential term on the direction of B is ignored, $R_\perp/R_\parallel$ is equal to the anisotropy of the wavefunction:

$$R_\perp(\beta)/R_\parallel(\beta) = |\psi_\parallel(r, \beta)|^2/|\psi_\perp(r, \beta)|^2$$

where $|\psi_\parallel|$ is the magnitude of ψ in the direction of the field, $|\psi_\perp|$ is the magnitude of ψ in the perpendicular direction and $r = L^*/2$. In table 2 the distance r, in units of a_0, derived from the numerical solution of the wavefunction (figure 6), is given for each sample at different β.

The resistance anisotropy does not support the view that L^* increases with increasing B. For the shortest mesa, r is almost constant, independent of β. For the two larger samples there is a small systematic decrease in r with increasing β. The same effect is apparent in the transverse magnetoresistance of the samples (figure 5). At high fields

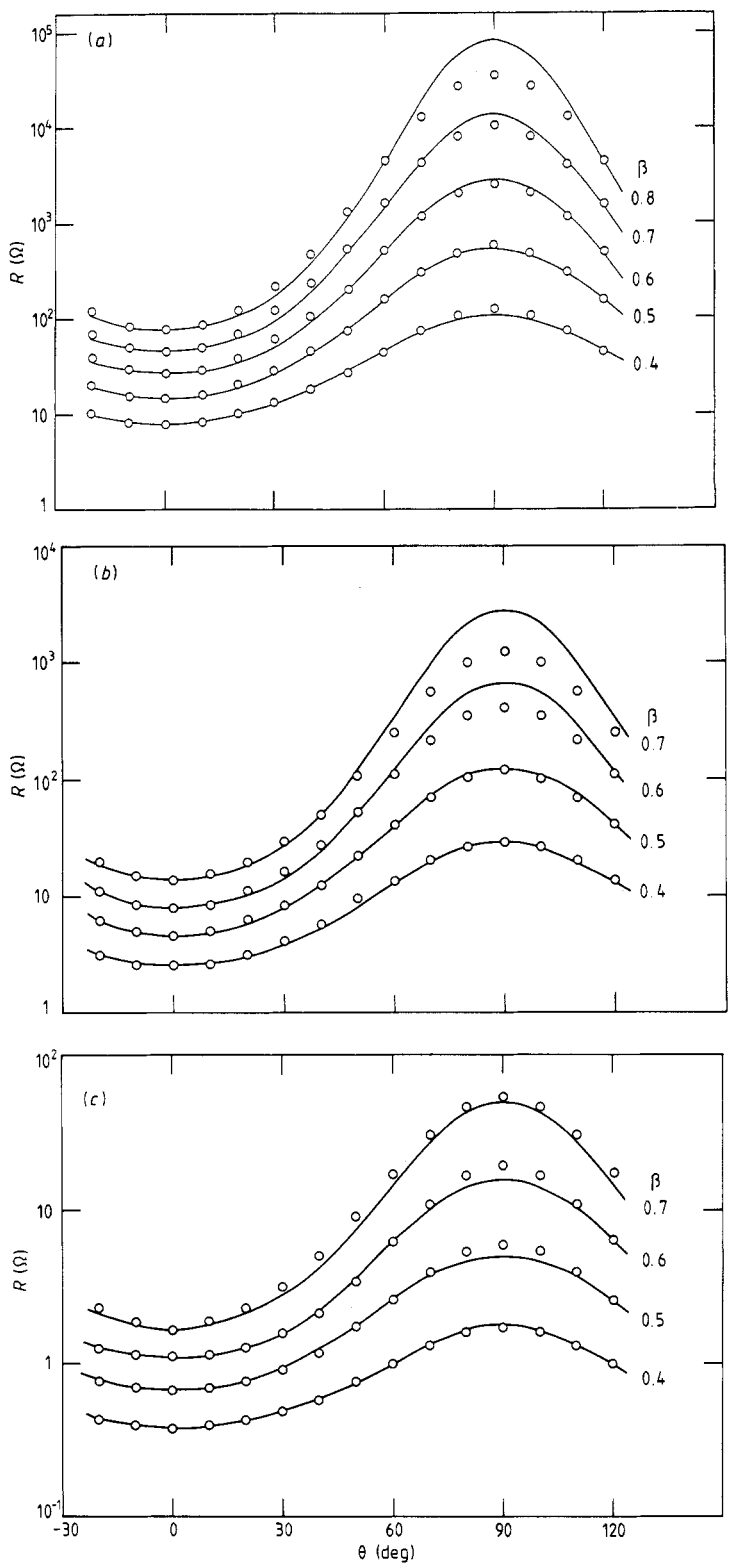

Figure 8. The resistance at various magnetic fields of the (*a*) $L = 128$ nm, (*b*) $L = 113$ nm and (*c*) $L = 97.5$ nm samples as a function of the angle θ between the current and magnetic field directions: ——, theoretical predictions using the numerical wavefunction.

Table 2. The distance r from the donor site, for which the anisotropy $|\psi_{\parallel}|^2/|\psi_{\perp}|^2$ is equal to the measured magnetoresistance anisotropy $R_{\perp}/R_{\parallel}$ of the samples.

		L = 129 nm		L = 113 nm		L = 97.5 nm	
β	B (T)	$R_{\perp}/R_{\parallel}$	r (units of a_0)	$R_{\perp}/R_{\parallel}$	r (units of a_0)	$R_{\perp}/R_{\parallel}$	r (units of a_0)
0.4	5.28	19.8	4.1	13.0	3.8	4.4	3.1
0.5	6.60	49.0	3.9	31.1	3.7	7.2	3.0
0.6	7.92	126.6	3.9	62.3	3.6	18.3	3.1
0.7	9.24	302.1	3.8	128.7	3.5	35.9	3.1
0.8	10.56	652.0	3.7	216.2	3.4	65.5	3.1

Table 3. The effective sample length L^* provides the best agreement between the angular dependence of $|\psi_{max}|^2$ and $R(\theta)$ for the three samples (figure 8). Here a_0 is taken to be 10 nm.

L (nm)	L^* (units of a_0)	L^* (nm)
129 ± 1	7.90 ± 0.3	79 ± 3
113 ± 1	7.45 ± 0.2	74.5 ± 2
97.5 ± 1	6.10 ± 0.1	61 ± 1

the sample resistance $R_{\perp}(B)$ falls below the theoretical curve derived for a fixed value of L^*. Although both trends are consistent with a decrease in L^*, a more plausible explanation is that a parallel conduction process, probably two-step hopping, is significant in the larger samples at high transverse magnetic fields.

The full curves in figure 8, with which $R(\theta)$ is compared, are derived from the angular shape of the wavefunction. The theoretical curves show the dependence of $|\psi_{max}|^{-2}$ on θ for a fixed sample length. For each value of θ it is necessary to find the maximum value of $|\psi|^2$ at the edge of the active layer. Since the surfaces of constant $|\psi|^2$ are approximately ellipsoidal, it is important to note that, except for $\theta = 0°$ and $\theta = 90°$, the largest value of ψ, for a donor situated in the centre of the n^- layer, occurs at an angle of less than θ with respect to the field direction and a distance $r > L^*/2$ from the donor site (figure 4). The length L^*, given in table 3, for which $|\psi_{max}(\theta)|^{-2}$ is derived, is chosen to be twice the mean value of r in the magnetic field range $\beta = 0.4$–0.6 shown in table 2. Good agreement is therefore ensured between $R_{\perp}/R_{\parallel}$ and the theoretical curves for the three lowest fields.

The agreement between $R(\theta)$ and $|\psi_{max}(\theta)|^{-2}$ for $\beta = 0.4$–0.6 is remarkably good for all three samples. At high fields ($\beta > 0.6$), the resistance of the two longer samples in the $\theta = 90°$ direction is less than the theoretical values, as expected from the curl-off in $R_{\perp}(B)$ (figure 5). The agreement between the experimental points and the theory is further demonstrated in figure 9.

The theoretical curves in figures 8 and 9 are scaled to agree with the experimental data at $\theta = 0°$. This adjustment is necessary because of the anomalously large longitudinal magnetoresistance discussed in section 5. The good agreement between the theoretical

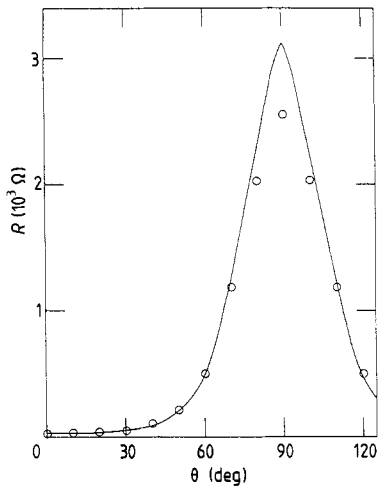

Figure 9. The magnetoresistance data in figure 8(*a*) for $\beta =$ 0.6 shown on a linear plot of resistance against angle.

and experimental curves implies that the scaling applied works for all θ. This in turn implies a magnetoresistance of the form

$$R(B) \propto R_0(B)\,|\psi_{\max}(L^*/2)|^{-2}$$

where $R_0(B)$ accounts for most of the longitudinal magnetoresistance and is independent of θ,

7. Discussion

We have shown that the angular dependence of the magnetoresistance of the very short mesas can be understood in terms of conduction via donor impurities located close to the middle of the n^- layer and that it is closely related to the shape of the donor wavefunction. In this section the assumptions made in our model are discussed and their likely effect on the agreement that we obtain between the theoretical curves and the measured sample resistance is assessed.

The transverse magnetoconductance (equation (9)) contains a pre-exponential term proportional to λ^2 and hence inversely proportional to B. This dependence on B is not present in the asymptotic expression for the wavefunction (equation (8)) but arises from the integration of the transition probabilities over the sample length (equation (6)). A similar, but much weaker, B-dependence is present in the longitudinal magnetoconductance through the magnetic-field-dependent Bohr radius (see equations (7) and (19)). The angular dependence of the conductance should, therefore, contain an extra pre-exponential B-dependence that varies with the field direction. The extra B-dependence is largest for the transverse case when the wavefunction falls most rapidly with increasing B. Since the numerical and analytical forms of the wavefunction are then similar, it is reasonable to assume a transverse magnetoconductance of the form

$$G_\perp \propto B^{-1}\,|\psi_{\max}|^2.$$

The calculated resistance, in the $\theta = 90°$ direction, in figure 8 would then be larger, by one order of magnitude in a field of 10 T. In the longitudinal direction the numerical

solutions of the wavefunction are less dependent on B than equations (7) and (19) suggest. Therefore the extra pre-exponential B-dependence is small and equation (21) is reasonable.

In our theoretical interpretation of impurity-assisted tunnelling, the transition rate for an electron tunnelling into, or out of, an impurity state is proportional to $|\psi_{max}|^2$. The probability of electrons tunnelling at other angles, where the transition rate is less, is assumed to increase, or decrease, in proportion to $|\psi_{max}|^2$. This would be true only if the shape of the wavefunction were uniform, i.e. spherical. In a magnetic field the wavefunction is distorted; the relative probability of an electron transition at angles other than the optimum will vary with the strength and direction of the field. The magnitude of this effect may be estimated by plotting $|\psi|^2$, for a donor in the centre of the active layer, along the n^+–n^- boundary.

Along the direction of the magnetic field the contours of constant $|\psi|^2$ in figure 6 may curve more sharply at higher B. Therefore the relative contribution to the current of electrons tunnelling at small angles to B is less and the magnetoresistance is larger. We find that the overlap of $|\psi|^2$ with the plane of the n^+–n^- boundary is reduced by a factor of 8 between 0 and 10.6 T for $L^* = 7.90a_0$. This compares with a reduction in $|\psi_{max}|^2$ by a factor of 2. Therefore, by including the three-dimensional aspect of the wavefunction, the predicted magnetoresistance rise for the largest sample is $R_\parallel(B = 10.6\,\mathrm{T})/R(B = 0\,\mathrm{T}) \simeq 8$. This is insufficient to explain the observed longitudinal magnetoresistance of this sample, $R_\parallel(B = 10.6\,\mathrm{T})/R(B = 0\,\mathrm{T}) \simeq 80$.

In the transverse direction the B-dependence of the overlap of $|\psi|^2$ with the n^+n^- boundary is well described by the variation in $|\psi_{max}|^2$. For $B = 5.3$ T the predicted resistance of the $L = 129$ nm sample is 20% larger if the whole wavefunction is considered than that given by the reduction in $|\psi_{max}|^2$ only; for $B = 9.3$ T the predicted resistance is 30% larger.

To evaluate the overlap of $|\psi|^2$ with the n^+–n^- boundary for all possible values of θ, L^* and B would be difficult. From this brief analysis, we find that the result would be to reduce the theoretical resistance anisotropy by a factor of about 8 for $L^* = 7.90a_0$ at $B = 10.6$ T. Inclusion of the extra angle-dependent term discussed earlier increases this anisotropy by about one order of magnitude. The scale of these two competing effects is small compared with the exponential variation in $|\psi_{max}|^2$ shown in figures 8 and 9.

To summarise, we have used the numerical solutions of the ground-state hydrogen-like wavefunction in strong magnetic fields of Rösner *et al* (1984) to interpret the angular dependence of the magnetoresistance of very short n^+–n^-–n^+ GaAs mesa samples. We find that, by substituting the solutions of Rösner *et al* (1984) into our simple impurity-assisted tunnelling model, good agreement can be obtained between the theoretical angular dependence of the magnetoresistance and our measurements. This agreement exists provided that the length of the potential barrier in our samples is assumed to be less than the thickness of the n^- layer as grown. The difference can be explained by screening effects at the boundaries between the n^+ and n^- regions.

A more detailed description of this work is contained in Roche (1988).

Acknowledgment

This work is supported by the Science and Engineering Research Council.

References

Buczko R, Chroboczek J A and Wunner G 1987 *Phil. Mag. Lett.* **56** 251
Emel'yanenko O V, Lagunova T S, Nasledov D N, Nedologo D D and Timchenko I N 1974 *Sov. Phys.–Semicond.* **7** 1280
Main P C, Roche I P, Eaves L, Owers-Bradley J R, Taylor D C, Singer K E, Hill G and Pate M A 1986 *Superlatt. Microstruct.* **2** 385
Roche I P 1988 *PhD Thesis* University of Nottingham
Rösner W, Wunner G, Herold H and Ruder H 1984 *J. Phys. B: At. Mol. Phys.* **17** 29
Shklovskii B I and Efros A L 1984 *Electronic Properties of Doped Semiconductors (Springer Series in Solid State Sciences 45)* (Berlin: Springer) p 160